Previous motor task performance impacts phase-based EEG resting-state connectivity states

Nils Rosjat[1], Maximilian Hommelsen[1], Gereon R. Fink[1,2], Silvia Daun[1,3,*]

1 Cognitive Neuroscience, Institute of Neuroscience and Medicine (INM-3), Forschungszentrum Jülich, Jülich, Germany
2 Medical Faculty, University Cologne, and Department of Neurology, University Hospital Cologne, Cologne, Germany
3 Institute of Zoology, University of Cologne, Cologne, Germany

* Corresponding author: s.daun@fz-juelich.de

Abstract

The resting human brain cycles through distinct states that can be analyzed using microstate analysis and electroencephalography (EEG) data. In this approach, multi-channel EEG scalp recordings are classified into spontaneously interchanging microstates based on topographic features. These microstates may be valuable biomarkers in neurodegenerative diseases since they reflect the resting brain's state. However, microstates do not provide information about the active neural networks during the resting-state.
This article presents an alternative and complementary method for analyzing resting-state EEG data and demonstrate its reproducibility and reliability. This method considers cerebral connectivity states defined by phase synchronization measured using the corrected imaginary phase-locking value (ciPLV) based on source-reconstructed EEG recordings. We analyzed resting-state EEG data from young, healthy participants acquired on five consecutive days before and after a motor task. We show that our data reproduce the microstates previously reported. In source connectivity space, we reveal four stable topographic patterns over the multiple recording sessions. Besides, while the classical microstates were unaffected by the preceding motor task, the connectivity states were altered reflecting suppression of frontal activity in the post-movement resting state.

Keywords— microstates, dynamic graphs, electroencephalography, motor task, neurological/psychiatric disease

Introduction

The state of the human brain at rest has been studied extensively using multichannel electroencephalography (EEG) and functional magnetic resonance imaging (fMRI), showing that the brain stays active in an organized manner to be prepared for unpredictable incoming stimuli (1–3). Based

on connectivity analyses, several networks have been identified, including the visual, sensory-motor, basal ganglia and default mode networks (4–7). In fMRI analyses, these networks are extracted by analyzing the correlations of BOLD signal fluctuations among various brain regions (4). However, the fluctuations found in these signals are generally too slow to be associated with preparations or responses to unpredictable stimuli.

On the other hand, analysis of EEG signals providing a much higher temporal resolution focuses on the correlation of fluctuations in amplitudes of oscillatory activity (8; 9). Several methods extract EEG signal information to analyze resting state networks. For example, the so-called microstate analysis is a well-established method that examines the topographical configuration of electrode potentials as measured at the scalp level. Four prototypical microstates, have been reliably identified (e.g. (10–12)), which spontaneously transition between each other within several hundreds of milliseconds and most likely reflect rapid switching between neural networks. For instance, pre-stimulus microstates have been shown to affect stimulus response performance, suggesting that EEG signals unravel the role of brain microstates when preparing for incoming stimuli (13). Although combined EEG-fMRI studies indicate that the EEG microstates are highly correlated with fMRI resting state networks (11), the neural mechanisms underlying microstate activity and their functional relevance remain elusive.

In this study we took an approach different from the microstate analysis to investigate the neural mechanisms underlying active brain networks at rest. For this, we aimed to define and analyze connectivity states underlying resting state networks using EEG resting-state data. We furthermore tested whether these networks are stable over several measurement days and whether they are affected by cognitive or motor tasks. Thus, we investigated whether the acquisition time point within an experiment, i.e., pre- or post-task performance, affected the resting-state connectivity states. We used source reconstruction methods to determine the source activity at any given time point and determined the sources' connectivity state using the corrected imaginary phase-locking values (ciPLV). This approach is to be distinguished from work by (14). In their study, the authors utilized microstates to parcellate the resting state timecourse into brainstates before conducting connectivity analysis on the microstates. In contrast, we compute resting-state connectivity in source space and cluster the obtained source networks into distinct groups, which we refer to as connectivity states. This approach enables us to examine the topographical organization of the source networks. It furthermore addresses previous concerns regarding the combination of microstate analysis and connectivity analysis, pointed out by (15). Thus, while previous literature aimed to inform connectivity analysis by microstate segmentation, we used a fundamental different approach and strive to provide a novel perspective on understanding EEG resting-state connectivity. We thus extend previous work by offering an alternative approach that enhances our understanding of the neural dynamics underlying resting-state brain activity.

Many studies have identified disruptions in specific microstate features (e.g., occurrences, durations) in neuropsychiatric disorders, including schizophrenia (16; 17), dementia (18), depression (19), Tourette's syndrome (20), or panic disorder (21). In contrast, data on stroke-related disruptions of microstates or active resting-state networks remain sparse. The source-localized connectivity-state approach presented here might help to understand better disturbed cortical network organization following a stroke. Before applying this method to patients, it is, however, mandatory to test whether the results in healthy subjects are stable across measurements and time.

Materials and methods

Participants

In this study, 27 healthy young subjects (11 female, age (mean ± sd): 27.9 years ± 3.4, range: 22-34 years) participated and received monetary compensation. Participants had normal or corrected-to-normal vision, no neurological or psychiatric disease history, were not under medication at any time, and had no cranial metallic implants. According to the Edinburgh Handedness Inventory (22), 22 participants were right-handed (score > 50), two were left-handed (score < -50), and three had intermediate scores. The study was approved by the Ethics Commission of the Faculty of Medicine, University of Cologne (ID: 14-006). All participants provided written informed consent before the start of the experiment.

After the application of all exclusion criteria (see below), datasets from 24 (of the 27) participants were used for statistical analysis.

Experimental Setup

For the visual representation of the experimental paradigm, the software Presentation (v. 20.2 Build 07.25.18, Neurobehavioral Systems, Inc.) was used. The behavioral responses of the subjects were recorded via an fMRI-compatible button pad (1-hand) system (LXPAD-1x5-10M, NAtA Technologies, Canada).

During the experiment, a 64-channel scalp EEG was recorded with active Ag/AgCl electrodes (actiCap, Brain Products GmbH, Germany). The electrodes were positioned in the standard 10-20 layout (ground AFz, reference on left mastoid). Three electrodes (FT9, FT10, TP10) were used for EOG recording. One electrode was placed under the left eye for vertical movements and one each near the left and right lateral canthi for horizontal movements. The recorded voltages were amplified during the measurements by a BrainAmp DC amplifier (Brain Products GmbH, Germany).

A stereotactic neuronavigation system (Brainsight v. 2.3, Rogue Research Inc., Canada) was used (for details see (23)) to ensure reliable positioning of the EEG electrodes over the multiple measurements taken on different days.

The experimental sessions took place in a controlled environment to ensure minimal external influences on the participants' resting state. The chamber used for the experiments was dark, sound-proof, and magnetically shielded. This setup aimed to minimize visual, auditory, and electromagnetic interferences that could potentially impact the resting-state measurements. During the experimental sessions, participants were seated in an upright position facing a computer screen.

Experimental Protocol and Paradigm

Subjects were each measured at identical times of the day for five consecutive days (Monday through Friday). For one subject, the fifth measurement had to be performed three days apart for technical reasons. For all subjects, each session (i.e., each measurement day) consisted of two resting-state measurements interrupted by a non-rest finger tapping task. Besides, a more complicated finger

movement sequence was recorded at the end of the session, which will not be considered further here.

The individual conditions were organized in detail as follows and together lasted for about 40 minutes.

1. Resting State (RS1):

   A white dot was shown in the center of the screen for the entire duration of 5 minutes. Subjects were instructed to keep their eyes open, fixating their gaze on the white dot. Further, it was emphasized that the subjects should relax, avoid movements as much as possible, and not think of anything specific. This task will be referred to as RS1.

2. Tapping Task (Tap):

   During this task, a white dot was also presented for fixation on the center of the screen. However, the dot faded in this task every 10-14 seconds. During this period, subjects had to press the button on the response pad with their left index finger as quickly and as often as possible until the dot reappeared on the screen. The entire block consisted of 60 movement periods (dot absent, Move) and 60 waiting periods (dot present, Wait) and lasted in total about 14 minutes.

3. Resting State (RS2):

   The second block of the Resting State (RS2) proceeded as the first.

4. Sequence Task (Sequence):

   In this task, the subjects had to press a given, more complex sequence as quickly and as often as possible with the fingers of one hand. This task will not be described in more detail here, as it will not be considered in the following analyses (see (23) for details).

Fig 1. Experimental Paradigm. Figure showing the experimental conditions. Top: Single measurement sequence consisting of 5 min Resting State (RS1), 14 min Tapping Task (Tap), 5 min Resting State (RS2), and finally, 14 min Sequence Task (Sequence). The sequence task is shown in grey as it will not be considered for further analysis; Bottom: Temporal sequence of measurements for days 1 to 5.

EEG Preprocessing

EEG preprocessing was performed using EEGLAB (24), integrated into MATLAB (R2016b, Mathwork Inc, Natick, MA). EEG source reconstruction was carried out using MNE-Python (v. 0.22) in Python (v. 3.8.8). Further analyses were performed using custom scripts also implemented in Python.

The continuously recorded data was first downsampled to a sampling frequency of 128 Hz. In the next step, the data were band-pass filtered to the frequency range 1-40 Hz with a Hamming windowed sinc FIR filter (i.e., high pass followed by low pass). The continuous recordings then underwent an

artifact correction process to remove oculomotor activity related to eye blinks and saccades based on the information from the EOG electrodes. Eyeblink removal was performed for each day separately on a copy of the data set following the procedure introduced by (25). ICA weights obtained from this procedure were transferred and applied to the original dataset. Independent components related to eyeblinks and saccades were identified using the automatic detection algorithm ADJUST (26), implemented as a plug-in for EEGLAB.

Following eyeblink correction, the original dataset underwent visual inspection to remove time-intervals and channels contaminated with artifacts. Signals of rejected channels were interpolated by using information from other channels using spherical spline interpolation. Time-intervals showing artificial behavior were cut out entirely from the data. All channels were then re-referenced to the Common Average Reference (27).

Data Quality Assessment

In order to ensure the quality of the data and minimize the potential influence of drowsiness on the resting state measurements, we carefully checked for any signs of decreased vigilance or wakefulness in the subjects. If epochs of drowsiness were identified, they were excluded from further analysis. This approach aimed to maintain the validity and reliability of the resting state measurements and minimize any confounding effects arising from decreased vigilance or wakefulness.

After preprocessing, we obtained 135 data sets (27 subjects x 5 days). All subjects completed at least the first three tasks, i.e., RS1, Tap, RS2 (see (23)). To be included in the final data analysis, at least 4 of the 5 subjects' data sets had to meet the following quality criteria:

1. Fewer than 7 excluded channels,
2. $> 180\,\mathrm{s}$ artifact-free RS1,
3. $> 180\,\mathrm{s}$ artifact-free RS2.

Of all 27 subjects, 24 met the above criteria and were included in the analyses reported below. Of these, 18 (of 24) had performed all 4 tasks, and the remaining 6 (of 24) had performed the first 3 tasks. The best 4 of the 5 sessions (days) were used from all subjects to ensure a comparable amount of data per subject. For subjects with 5 good sessions, the first day of each measurement was excluded.

Microstate analysis

We determined classical microstates at the electrode level for face validity before analyzing the source activity. For this purpose, we used the MNE Microstates Toolbox (28). Analogously to the literature, the continuous recordings at the electrode level were divided into 4 states by applying the k-means algorithm with $k = 4$, each with 10 different initializations per subject and measurement. The best of the 10 fits for each subject was used to determine the 4 common group centroids.

Source localization

The continuous recordings were projected from the electrode onto the source space using dynamic statistical parametric mapping (dSPM) (29). Afterwards, the norm of the source orientations was taken (30). We applied methods from FreeSurfer for source-space reconstructions (31; 32). As no individual MRIs were available for the subjects, source data were mapped onto FreeSurfer's "fsaverage" common template source space. Source locations were then grouped into 150 parcels according to the Destrieux Atlas (33). For each parcel, one common, i.e., shared, parcel time course was extracted by finding the dominant direction of the source space normal vector orientations within each parcel. Each time series at vertices whose orientation is more than 180° different from the major direction underwent a sign-flip. Finally, all vertices within each parcel were averaged to produce the final common source time course. Source localization was performed on the movement data first to ensure the proper functioning of the algorithm as sources are known in this condition.

Network construction

Following source localization, we transformed the continuous source time courses of the resting state data to the time-frequency domain using Morlet wavelets (34). We focused our analysis on the alpha frequency range (8-12 Hz), i.e., a typical choice in EEG microstate literature (e.g., (35)), and applied a step size of 0.5 Hz. The choice of the alpha frequency band was based on several reasons outlined below:

1. Connectivity analysis: It is necessary to narrow down the frequency range of interest for phase connectivity analysis. Broadband approaches may not be suitable for capturing specific connectivity patterns effectively. By focusing on the alpha band, we aimed to target a specific frequency range that is known to exhibit meaningful connectivity patterns.

2. Microstate analysis: Previous studies utilizing classical microstate analysis have reported consistent states for alpha filtered data during resting state measurements. This provides a foundation for investigating the potential role of alpha oscillations in our study.

3. Importance for motor networks: The alpha band is relevant for motor networks (36; 37). By focusing on the alpha band, we aimed to explore potential connectivity patterns and network dynamics specific to motor-related brain regions.

4. Technical constraints: In our study, we faced technical constraints that influenced our choice of frequency boundaries. Lowering the frequency boundary would have resulted in decreased time-resolution, which would have hindered our ability to capture fine-grained temporal dynamics and connectivity changes.

By narrowing our focus to the alpha band, we aimed to balance between the methodological requirements of the connectivity analysis, the existing literature on alpha oscillations, the relevance of the alpha band to motor networks, and technical considerations associated with our data processing pipeline.

The Morlet wavelet cycles were set to increase from 4 at the lower-frequency boundary to 6 at the upper-frequency boundary. After the time-frequency transformation, we extracted the time courses of the amplitudes and phases for each frequency. We quantified the connectivity between two different parcels (regions) by synchronization determined by the single-trial corrected imaginary phase-locking value (ciPLV; (38)). As we used continuous data without any stimulus onset or

reoccurring trials, we followed the suggestion by Lachaux et al. (39) and computed the phase-locking over a specific period instead of trial-wise phase-similarity. Thus, two parcels are defined as being connected if the phase difference remains constant over this period. In our analysis, this period was set to 300 ms. For a pair of parcels m and n, ciPLV is defined as:

$$\text{ciPLV} = \frac{\frac{1}{T}\,\text{Im}\left(\sum_{t=1}^{T}\exp(i(\varphi_k(t)-\varphi_j(t)))\right)}{\sqrt{1-\left(\frac{1}{T}\,\text{Re}\left(\sum_{t=1}^{T}\exp(i(\varphi_k(t)-\varphi_j(t)))\right)\right)^2}}$$

Here φ_k(t) denotes the phase of the source reconstructed EEG signal at parcel k at time point t. T is the total number of time points in the 300 ms interval. To obtain a time-dependent connectivity measure, the ciPLV is computed in a sliding window approach. Previous literature (e.g., (35)) has shown microstates to be stable for predominantly 100 ms before transitioning to the next state. Thus, the windows were set to have a 200 ms overlap to achieve a time resolution of 100 ms. While minimum ciPLV = 0 represents a random distribution of phase difference over the whole time interval, a maximal ciPLV = 1 occurs only in the case of perfect phase locking of the phase differences with a phase difference of $\pi/2$. Connectivity with zero-phase lag is intentionally removed from the analysis by the specific selection of ciPLV as the connectivity measure since it is, to a high degree, artificially created by source leakage.

Fig 2. Connectivity State Pipeline. Representation of how the connectivity states were determined. Top row (left): extraction of source activity for two parcels, m and n; bottom row (left): computation of the ciPLV connectivity metric; bottom row (middle): graph construction for each time window by thresholding the ciPLV; top row (right): depiction of the resulting dynamic graph networks; bottom row (right): application of k-means clustering for connectivity state assignment.

The connectivity analysis classifies pairs of parcels at each time window into those with higher and lower degrees of synchronization. In the following, we will focus on the 10% strongest connections at each given time window with a resolution of 100 ms. By doing so, we can define a binary undirected graph $G_t = (V, E_t)$, where the graph G is defined by a set of vertices V, i.e., the source locations, and edges $E_t : V \times V \rightarrow R$, i.e., the strongest connections at each time window. The dynamic graph, also called a dynamic network, is then defined as an ordered set of graphs $G(t) = \{G_t | t \in [1, \cdots, T_{tot}]\}$. Here, T_{tot} denotes the total amount of artifact-free resting state data for a given participant. The use of dynamic graphs is crucial here, as they account for time-varying connectivity patterns that are necessary to determine the time-evolving formation of subnetworks that a static network could not unravel.

Connectivity State Clustering

For clustering the connectivity patterns into different connectivity states, we used a similar approach as described above for the microstate analysis. First, we determined 4 different connectivity states by applying the k-means clustering algorithm on the full dataset of 24 subjects and 4 sessions (RS1 and RS2). Additionally, we used the elbow method (40; 41) to determine the optimal number k

for the k-means algorithm. This approach led to 8 connectivity states, which we computed for all subjects (24), sessions (days 1-4), and tasks (RS1, RS2). In the following, we focus on the number of 4 clusters typically used in the resting state EEG literature (e.g., (10–12; 42)). Results for the 8 clusters can be found in the Supplementary Material.

Statistical Analysis

The duration of the micro- and the connectivity states within each RS measurement were compared using pairwise t-tests over individual subjects and measurement days. For further comparisons of the effects of measurement sessions (days $1-4$) or pre- and post-motor performance RS (RS1 vs. RS2), we performed additional pairwise t-tests for each connectivity state.

Results

Microstate Analysis

In the first step, we performed a classical microstate analysis of the resting-state data (RS1 and RS2). We chose $k = 4$ clusters to match previous results reported in the literature (10). We added this step to our analyses to reproduce existing microstate results and investigate the variability of these results over multiple measurement sessions on different days. Further, we tested whether the performance of a motor task before a resting state influences the microstates.

Fig 3. Microstate Figure. A: Scalp microstate topographies (note: polarities are to be neglected), B: relative time the brain stays in each state, C: transitions between the four microstates displayed as a Markov diagram (A-C: all subjects, all sessions, RS1 only), D: comparison of RS1 and RS2 state durations (all subjects, all sessions).

In Fig. 3A, we show the four microstates determined from our dataset. The four states exhibit the same basic topographies as have been reported by many studies in the previous literature (10–12). The four microstates found in our data are characterized topographically by (i) a diagonal polarity shift from left parietal to right frontal regions (MS A), (ii) a mirrored diagonal polarity shift from the right parietal to left frontal regions (MS B), (iii) an occipital polarity shift (MS C), and a polarity shift at the central electrodes (MS D). When separating the sessions into pre-task (RS1) and post-task (RS2) resting states, there were no apparent changes in the four microstates (see Supplementary Material). Similarly, the microstates remained stable when comparing the different measurement days (session 1 to session 4; see Supplementary Material). Analysis of the duration of the four microstates showed no significant difference between all four microstates (Fig. 3B). When looking at the transition between the four microstates, we can see that each state had a high probability ($> 50\,\%$) of staying in the same state while transitions to the other states were evenly distributed at roughly $15\,\%$ (Fig. 3C). Thus, there existed no preferred microstate at the scalp level and no clear order of state transitions.

The overall picture remained unchanged when comparing the occurrences of microstates between RS1 and RS2 (Fig. 3D). The frequency of each microstate is in the range of 20% to 30%. A statistical comparison also revealed no significant differences for state B (RS1: $23.78\% \pm 2.86$, RS2: $23.92\% \pm 2.44$, $p > 0.05$, $t = -0.545$, $df = 95$) and for state C (RS1: $24.98\% \pm 4.44$, RS2:

26.14%$\pm$3.27, $p > 0.05$, $t = -1.834$, df = 95). However, the other two states showed slight differences between RS1 and RS2. While state A was significantly increased in RS2 (RS1: 24.48% $\pm$ 2.54, RS2: 26.44% $\pm$ 2.94, $p < 0.0001$, $t = -6.812$, df = 95), state D was less frequent in RS2 (RS1: 26.77% $\pm$ 3.26, RS2: 23.50% $\pm$ 3.98, $p < 0.0001$, $t = 5.621$, df = 95).

Source Connectivity Analysis

ciPLV on Source Level After transforming the scalp-recorded EEG data to source-localized activity using dSPM implemented in MNE-Python (30), we extracted source activity from 150 parcels as defined by the Destrieux atlas (33). The proper functioning of the source localization and reasonable selection of the parcellation was ensured by using the tapping condition as ground truth for source activity (see Supplementary Material, Fig. S3). We applied a sliding window approach for the source connectivity analyses in RS1 and RS2. The mean connectivity over all subjects and sessions ranged from 0.3 to 0.6 for the different pairs of source parcels (see Supplementary Material, Fig. S4). This non-zero source space phase-connectivity was utilized in the following to construct the networks that defined the source connectivity states of the resting brain.

Connectivity State Analysis According to the number of microstates on the scalp level found here and in previous studies, we decided to set the number of clusters to $k = 4$. Additionally, we defined $k = 8$ connectivity states determined by the elbow method (Results are shown in Supplementary Material, Fig. S2).

When displaying the centroids of the clusters as circular connectivity networks and mapping them onto a 3D image of the brain, the representations resemble those of the scalp topographies of the microstate analysis (Fig. 4). The four clusters can be described as (i) a diagonal connectivity pattern of left-frontal regions (CS A), (ii) a mirrored diagonal connectivity pattern of right-frontal regions (CS B), (iii) a parietal connectivity pattern (CS C), and (iv) a weaker all-to-all connectivity pattern (CS D; max 0.1 compared to 0.2-0.35).

Fig 4. Source Connectivity States. Top: circular presentation of source connectivity (the 10% strongest connections are shown) presenting parcels on each hemisphere on the left and right side of the circular plot, frontal parcels at the top, and occipital parcels on the bottom; Bottom: presentation of the involved parcels mapped onto the brain using the same color code as in the circular plot.

In the following, we investigated the duration of each connectivity state in the whole dataset, i.e., across all participants and measurement days. For roughly 55% of the time, the RS network remained in connectivity state D, whose occurrence was significantly increased compared to the other connectivity states (CS A: 14.86 $\pm$ 1.75 vs. CS D: 57.65 $\pm$ 2.49, df=95, t=-115.42, p $<$ 0.0001; CS B: 10.79 $\pm$ 1.3 vs. CS D: 57.65 $\pm$ 2.49, df=95, t=-134.56, p $<$ 0.0001; CS C: 16.69 $\pm$ 2.46 vs. CS D: 57.65 $\pm$ 2.49, df=95, t=-96.31, p $<$ 0.0001). Furthermore, CS B was significantly reduced compared to CS A (CS A: 14.86 $\pm$ 1.75 vs. CS B: 10.79 $\pm$ 1.3, df=95, t=26.30, p $<$ 0.0001) and CS C (CS C: 16.69 $\pm$ 2.46 vs. CS B: 10.79 $\pm$ 1.3, df=95, t=18.20, p $<$ 0.0001). There was no significant difference for the other connectivity states (Fig. 5A). The states switched between CS A - CS C only about $6 - 10\%$ but preferably first went back to CS D with a chance of $35 - 39\%$. This means that the connectivity state D served as some transition state having overall a lower connectivity (Fig. 5B).

Fig 5. Durations and Transitions of Source Connectivity States. A: A violin plot showing the source connectivity state durations for CS A (blue), CS B (green), CS C (red), and CS D (orange) in RS1. All significant differences are marked with an asterisk; B: graph displaying the transitions between the connectivity states.

When separating the data for the multiple measurement days (session 1 through session 4), the same distribution between the different connectivity states could be observed (Fig. 6). Statistically, there were no significant differences (ps > 0.05).

Fig 6. Connectivity States for multiple measurement days. A violin plot showing the source connectivity state durations for separate measurement days, i.e., sessions.

Another question we wanted to answer was whether the performance of a motor task before the resting state influences the identified connectivity states. Therefore, we compared the resting-state networks obtained from RS1 before the motor task performance to RS2 after the motor task performance. Here, CS A - CS D distributions deviated significantly between RS1 and RS2 (Fig. 7A). In contrast to the results for RS1 presented above, the duration of CS C was significantly increased (RS1: 16.69 ± 2.46, RS2: 42.7 ± 14.56, df = 95, t=-15.967, p< 0.0001) while the durations of the states CS A (RS1: 14.86 ± 1.76, RS2: 11.39 ± 4.53, df = 95, t=6.756, p< 0.0001), CS B (RS1: 10.79 ± 1.3, RS2: 8.75 ± 3.35, df = 95, t=5.6, p< 0.0001) and CS D (RS1: 57.65 ± 2.49, RS2: 37.15 ± 10.56, df = 95, t=18.623, p< 0.0001) were significantly reduced. The significant difference between CS C and CS D in RS1 reported above vanished in RS2, while the duration of CS C was significantly increased compared to CS A in RS2 (CS A: 11.39 ± 4.53, CS C: 42.7 ± 14.56, df=95, t=-16.89, p< 0.0001). The significant increase of CS C compared to CS B, as seen in RS1, remained present in RS2 (CS B: 8.75 ± 3.35, CS C: 42.7 ± 14.56, df=95, t=-19.75, p< 0.0001). A separate analysis of RS2 for the different measurement sessions revealed that the effect described above was stable and not driven by a single session (Fig. 7B). There were no significant differences for the CS durations in different measurement sessions. The state duration of CS A in session 3 was slightly decreased compared to sessions 1 (Ses1: 11.87 ± 4.78, Ses3: 10.4 ± 3.5, df=23, t=2.76, p= 0.011) and 4 (Ses4: 11.89 ± 4.94, Ses3: 10.4 ± 3.5, df=23, t=2.45, p= 0.023). However, after Bonferroni correction for multiple comparisons, those differences did not remain significant.

Fig 7. Task-dependent changes in the connectivity states. A: A violin plot showing the source connectivity state durations separately for RS1 and RS2 (all sessions); B: Stability of source connectivity state durations in RS2 for multiple measurement sessions.

Discussion

In this study, we conducted a source connectivity state analysis in a cohort of 24 young and healthy participants. While we performed a classical microstate analysis first, we focused not on directly comparing the scalp-level microstates and the source-level connectivity states but on elucidating underlying active neural networks during resting-state using both methods. Furthermore, we wanted to establish a methodological approach that demonstrates the reproducibility and reliability of

the presented method. This emphasis on methodological validation lays the ground for future applications, particularly clinical studies.

It is crucial to note that the analysis of both sensor and source space data, despite being different numerical transformations of the same underlying data set, provides valuable insight. In particular, we gain insights into how global patterns of resting-state activity manifest at a localized level, potentially uncovering unique features and relationships that are not readily apparent from scalp-level analysis alone (43).

By establishing the connectivity state analysis and including individual structural MRIs in the source reconstruction pipeline, we anticipate this to be particularly relevant in studies of stroke patients. In particular, the ability to define individual connectivity patterns on a single-subject source space level holds promise for future investigations of stroke patients. Such applications allow elucidating a lesion's impact on the resting-state networks and potentially inform personalized treatment and rehabilitation strategies.

Microstate analysis We performed a classical microstate (MS) analysis and found a set of four MS that matched previously reported classes (e.g. (10–12)). Interestingly, we did not find any significant differences between the durations or the transitions of the MS (Fig. 3 B-C). Furthermore, the MS were stable over multiple measurement days (Fig. S2).

Connectivity state analysis After source localization of the recordings of RS1 and RS2, the continuous resting state data were clustered into epochs of four distinct connectivity states (CS). When comparing the CS with the MS topographically, we observed that both the MS based on scalp data and the CS based on source reconstructed connectivity networks showed similar configurations, i.e., two states with a left frontal - right parietal diagonal separation and right frontal - left parietal separation, respectively, and a state with an occipitally centered separation. The last state defined by both approaches revealed a polarity change at central electrodes in the MS, reflected by a state of all-to-all connectivity with lower connectivity strength in the CS (Fig. 4).

Given the choice of the alpha-frequency range for the analyses (see Materials and Methods), one might assume that there may be an artificially increased tendency for occipital connections as occipital alpha is dominant in resting-state EEG (44). However, our results showed the brain's preference to stay in the state of intermediate all-to-all connectivity (CS D), which we called the transition state. The transitions between the states supported this view. There were only a few cases in which the resting brain switched between states CS A, CS B, or CS C directly. The most frequent way to get from one state of higher connectivity to another, i.e., switch between CS A, CS B, or CS C, was to first transition to state CS D, i.e., continuously lowering overall connectivity. Thus, all states showed the highest transition probability towards connectivity state D, while the transitions back to the other states from CS D were evenly distributed. This result was stable over the multiple measurement sessions. A similar transition pattern of brain states has been reported by (45). In fMRI data analyzed with Bayesian switching dynamical systems models, which estimated the probability distribution of the system's state based on differential equations using Bayesian statistics, they showed that states related to high cognitive load or fixation only were not suddenly shifting to one another, but first accessed states associated with an intermediate demand (45).

Differences induced by a motor task By including a finger-tapping task in our study, we investigated the differences in MS and CS induced by a motor task. Even though the influence on the MS duration was significant, the change induced by the task was relatively small (MS A increased

by 2%, MS D reduced by 3%). All four states were almost evenly distributed, with 25% duration in both RS1 and RS2. In the CS, the change in the duration of the states was much more accentuated. The duration of CS C significantly increased by more than 25%, while all other states, especially CS D (by more than 20%), decreased significantly. The significantly reduced CS D may be related to the default mode network (46) or parts of the cognitive control network (11), which supports the view that CS D may serve as a transition state. MS C, on the other hand, is commonly assumed to be related to the dorsal attention network (11; 46). According to (47), MS C might reflect reflexive aspects of attention, as subjects underwent a lengthy motor task after which they tried to relax without focusing on the previous motor task. Assuming connectivity state C represents a similar function as microstate C, increasing this connectivity state could represent an equivalent shift of attention. Besides, the switch to a resting state after motor task performance might reflect the suppression of fronto-central activity involved in motor planning and execution (48). Furthermore, the dorsal attention network modulates the visual network (49). The frequent change of visual information presented in the motor task, which was used to inform the subjects when to start and end the finger-tapping movements, was removed in RS2. During the finger-tapping condition, the subjects had to focus on the visual input to perform the motor task. As this attentional demand was removed in RS2, an activity change of the dorsal attention network may have resulted. We assume that the reduction of these parts of the default mode network in favor of the dorsal attention network reflects a shift from the activated motor state to a resting state and thus leads to a shift in the dorsal attention network in contrast to the pre-motor task resting-state condition.

Importantly, our data suggest that resting-state data before and after task performance should be analyzed strictly separately.

Reproducibility In the literature, many articles have reported a change in MS features (e.g., duration, occurrences, transitions) due to neuropsychiatric disease (16–21). In order to extend MS analysis to include CS of the resting brain, we aimed to show that the observed effects are stable across multiple days. We, therefore, split the recordings into four measurement days and tested the distribution of state durations in a paired t-test design. The results showed no significant differences within the subjects for multiple sessions. This finding suggests a reliable metric that can be applied in other subject populations to test for changes in CS features due to neurological disorders. For future research, e.g. in a clinical setting, this is a crucial step to provide reliable and stable results for subjects measured on different measurement days.

Acknowledgments

This work was funded by the Deutsche Forschungsgemeinschaft (DFG, German Research Foundation) — Project-ID 431549029, SFB 1451, and 491111487. We thank Hannah Kirsten, Alexandra Kurganova and members of the INM-3 for their valuable assistance in data acquisition.

Conflict of Interest Statement

The authors declare no competing financial interests.

Data Availability Statement

The data that support the findings of this study are openly available in Jülich-DATA at https://doi.org/10.26165/JUELICH-DATA/PV2LY1.

References

[1] Michael D Fox and Marcus E Raichle. Spontaneous fluctuations in brain activity observed with functional magnetic resonance imaging. *Nature reviews neuroscience*, 8(9):700–711, 2007.

[2] Michael D Fox, Abraham Z Snyder, Justin L Vincent, Maurizio Corbetta, David C Van Essen, and Marcus E Raichle. The human brain is intrinsically organized into dynamic, anticorrelated functional networks. *Proceedings of the National Academy of Sciences*, 102(27):9673–9678, 2005.

[3] Michael D Greicius, Ben Krasnow, Allan L Reiss, and Vinod Menon. Functional connectivity in the resting brain: a network analysis of the default mode hypothesis. *Proceedings of the National Academy of Sciences*, 100(1):253–258, 2003.

[4] Bharat Biswal, F Zerrin Yetkin, Victor M Haughton, and James S Hyde. Functional connectivity in the motor cortex of resting human brain using echo-planar mri. *Magnetic resonance in medicine*, 34(4):537–541, 1995.

[5] Christian F Beckmann, Marilena DeLuca, Joseph T Devlin, and Stephen M Smith. Investigations into resting-state connectivity using independent component analysis. *Philosophical Transactions of the Royal Society B: Biological Sciences*, 360(1457):1001–1013, 2005.

[6] Marilena De Luca, Christian F Beckmann, Nicola De Stefano, Paul M Matthews, and Stephen M Smith. fmri resting state networks define distinct modes of long-distance interactions in the human brain. *Neuroimage*, 29(4):1359–1367, 2006.

[7] Jonathan D Power, Alexander L Cohen, Steven M Nelson, Gagan S Wig, Kelly Anne Barnes, Jessica A Church, Alecia C Vogel, Timothy O Laumann, Fran M Miezin, Bradley L Schlaggar, et al. Functional network organization of the human brain. *Neuron*, 72(4):665–678, 2011.

[8] Francesco De Pasquale, Stefania Della Penna, Abraham Z Snyder, Christopher Lewis, Dante Mantini, Laura Marzetti, Paolo Belardinelli, Luca Ciancetta, Vittorio Pizzella, Gian Luca Romani, et al. Temporal dynamics of spontaneous meg activity in brain networks. *Proceedings of the National Academy of Sciences*, 107(13):6040–6045, 2010.

[9] Pascal Fries. Rhythms for cognition: communication through coherence. *Neuron*, 88(1):220–235, 2015.

[10] Thomas Koenig, Dietrich Lehmann, Marco CG Merlo, Kieko Kochi, Daniel Hell, and Martha Koukkou. A deviant eeg brain microstate in acute, neuroleptic-naive schizophrenics at rest. *European archives of psychiatry and clinical neuroscience*, 249(4):205–211, 1999.

[11] Juliane Britz, Dimitri Van De Ville, and Christoph M Michel. Bold correlates of eeg topography reveal rapid resting-state network dynamics. *Neuroimage*, 52(4):1162–1170, 2010.

[12] Arjun Khanna, Alvaro Pascual-Leone, and Faranak Farzan. Reliability of resting-state microstate features in electroencephalography. *PloS one*, 9(12):e114163, 2014.

[13] Sara Spadone, Pierpaolo Croce, Filippo Zappasodi, and Paolo Capotosto. Pre-stimulus eeg microstates correlate with anticipatory alpha desynchronization. *Frontiers in Human Neuroscience*, 14:182, 2020.

[14] Florian Hatz, Martin Hardmeier, Habib Bousleiman, Stephan Rüegg, Christian Schindler, and Peter Fuhr. Reliability of functional connectivity of electroencephalography applying microstate-segmented versus classical calculation of phase lag index. *Brain connectivity*, 6(6):461–469, 2016.

[15] Thomas Koenig and Pedro A Valdés-Sosa. Results obtained by combining different estimators of eeg connectivity become uninterpretable if the underlying models are incompatible. *Brain connectivity*, 8(2):57–59, 2018.

[16] Kyungwon Kim, Nguyen Thanh Duc, Min Choi, and Boreom Lee. Eeg microstate features for schizophrenia classification. *PloS one*, 16(5):e0251842, 2021.

[17] Fanglan Wang, Khamlesh Hujjaree, and Xiaoping Wang. Electroencephalographic microstates in schizophrenia and bipolar disorder. *Frontiers in Psychiatry*, 12:638722, 2021.

[18] Keiichiro Nishida, Yosuke Morishima, Masafumi Yoshimura, Toshiaki Isotani, Satoshi Irisawa, Kay Jann, Thomas Dierks, Werner Strik, Toshihiko Kinoshita, and Thomas Koenig. Eeg microstates associated with salience and frontoparietal networks in frontotemporal dementia, schizophrenia and alzheimer's disease. *Clinical neurophysiology*, 124(6):1106–1114, 2013.

[19] WK Strik, T Dierks, T Becker, and D Lehmann. Larger topographical variance and decreased duration of brain electric microstates in depression. *Journal of Neural Transmission/General Section JNT*, 99(1):213–222, 1995.

[20] A Stevens, W Günther, W Lutzenberger, M Bartels, and N Müller. Abnormal topography of eeg microstates in gilles de la tourette syndrome. *European Archives of Psychiatry and Clinical Neuroscience*, 246(6):310–316, 1996.

[21] Mitsuru Kikuchi, Thomas Koenig, Toshio Munesue, Akira Hanaoka, Werner Strik, Thomas Dierks, Yoshifumi Koshino, and Yoshio Minabe. Eeg microstate analysis in drug-naive patients with panic disorder. *PloS one*, 6(7):e22912, 2011.

[22] Richard C Oldfield. The assessment and analysis of handedness: the edinburgh inventory. *Neuropsychologia*, 9(1):97–113, 1971.

[23] Maximilian Hommelsen, Shivakumar Viswanathan, and Silvia Daun. Robustness of individualized inferences from longitudinal resting state eeg dynamics. *European Journal of Neuroscience*, 2022.

[24] Arnaud Delorme and Scott Makeig. Eeglab: an open source toolbox for analysis of single-trial eeg dynamics including independent component analysis. *Journal of neuroscience methods*, 134(1):9–21, 2004.

[25] Irene Winkler, Stefan Debener, Klaus-Robert Müller, and Michael Tangermann. On the influence of high-pass filtering on ica-based artifact reduction in eeg-erp. In *2015 37th Annual International Conference of the IEEE Engineering in Medicine and Biology Society (EMBC)*, pages 4101–4105. IEEE, 2015.

[26] Andrea Mognon, Jorge Jovicich, Lorenzo Bruzzone, and Marco Buiatti. Adjust: An automatic eeg artifact detector based on the joint use of spatial and temporal features. *Psychophysiology*, 48(2):229–240, 2011.

[27] Dennis J McFarland, Lynn M McCane, Stephen V David, and Jonathan R Wolpaw. Spatial filter selection for eeg-based communication. *Electroencephalography and clinical Neurophysiology*, 103(3):386–394, 1997.

[28] Marijn van Vliet. Mne-microstates. `https://github.com/wmvanvliet/mne_microstates`, 2022.

[29] Anders M Dale, Arthur K Liu, Bruce R Fischl, Randy L Buckner, John W Belliveau, Jeffrey D Lewine, and Eric Halgren. Dynamic statistical parametric mapping: combining fmri and meg for high-resolution imaging of cortical activity. *neuron*, 26(1):55–67, 2000.

[30] Alexandre Gramfort, Martin Luessi, Eric Larson, Denis A. Engemann, Daniel Strohmeier, Christian Brodbeck, Roman Goj, Mainak Jas, Teon Brooks, Lauri Parkkonen, and Matti S. Hämäläinen. MEG and EEG data analysis with MNE-Python. *Frontiers in Neuroscience*, 7(267):1–13, 2013.

[31] Anders M Dale, Bruce Fischl, and Martin I Sereno. Cortical surface-based analysis: I. segmentation and surface reconstruction. *Neuroimage*, 9(2):179–194, 1999.

[32] Bruce Fischl, Martin I Sereno, and Anders M Dale. Cortical surface-based analysis: Ii: inflation, flattening, and a surface-based coordinate system. *Neuroimage*, 9(2):195–207, 1999.

[33] Christophe Destrieux, Bruce Fischl, Anders Dale, and Eric Halgren. Automatic parcellation of human cortical gyri and sulci using standard anatomical nomenclature. *NeuroImage*, 53(1):1–15, 2010.

[34] Richard Kronland-Martinet, Jean Morlet, and Alexander Grossmann. Analysis of sound patterns through wavelet transforms. *International journal of pattern recognition and artificial intelligence*, 1(02):273–302, 1987.

[35] Dietrich Lehmann, Hisaki Ozaki, and Ivan Pál. Eeg alpha map series: brain micro-states by space-oriented adaptive segmentation. *Electroencephalography and clinical neurophysiology*, 67(3):271–288, 1987.

[36] Gert Pfurtscheller. Functional brain imaging based on erd/ers. *Vision research*, 41(10-11):1257–1260, 2001.

[37] Marie-Pierre Deiber, Etienne Sallard, Catherine Ludwig, Catherine Ghezzi, Jérôme Barral, and Vicente Ibañez. Eeg alpha activity reflects motor preparation rather than the mode of action selection. *Frontiers in integrative neuroscience*, 6:59, 2012.

[38] Ricardo Bruña, Fernando Maestú, and Ernesto Pereda. Phase locking value revisited: teaching new tricks to an old dog. *Journal of neural engineering*, 15(5):056011, 2018.

[39] Jean-Philippe Lachaux, Eugenio Rodriguez, Michel Le Van Quyen, Antoine Lutz, Jacques Martinerie, and Francisco J Varela. Studying single-trials of phase synchronous activity in the brain. *International Journal of Bifurcation and Chaos*, 10(10):2429–2439, 2000.

[40] Robert L Thorndike. Who belongs in the family. In *Psychometrika*. Citeseer, 1953.

[41] MA Syakur, BK Khotimah, EMS Rochman, and Budi Dwi Satoto. Integration k-means clustering method and elbow method for identification of the best customer profile cluster. In *IOP conference series: materials science and engineering*, volume 336, page 012017. IOP Publishing, 2018.

[42] Verena Brodbeck, Alena Kuhn, Frederic von Wegner, Astrid Morzelewski, Enzo Tagliazucchi, Sergey Borisov, Christoph M Michel, and Helmut Laufs. Eeg microstates of wakefulness and nrem sleep. *Neuroimage*, 62(3):2129–2139, 2012.

[43] Sima Azizi, Daniel B Hier, and Donald C Wunsch. Schizophrenia classification using resting state eeg functional connectivity: source level outperforms sensor level. In *2021 43rd Annual International Conference of the IEEE Engineering in Medicine & Biology Society (EMBC)*, pages 1770–1773. IEEE, 2021.

[44] Michael J Aminoff. *Aminoff's electrodiagnosis in clinical neurology*. Elsevier Health Sciences, 2012.

[45] Jalil Taghia, Weidong Cai, Srikanth Ryali, John Kochalka, Jonathan Nicholas, Tianwen Chen, and Vinod Menon. Uncovering hidden brain state dynamics that regulate performance and decision-making during cognition. *Nature communications*, 9(1):1–19, 2018.

[46] Benjamin A Seitzman, Malene Abell, Samuel C Bartley, Molly A Erickson, Amanda R Bolbecker, and William P Hetrick. Cognitive manipulation of brain electric microstates. *Neuroimage*, 146:533–543, 2017.

[47] Patricia Milz, Roberto D Pascual-Marqui, Peter Achermann, Kieko Kochi, and Pascal L Faber. The eeg microstate topography is predominantly determined by intracortical sources in the alpha band. *Neuroimage*, 162:353–361, 2017.

[48] Marcel Brass and D Yves Von Cramon. The role of the frontal cortex in task preparation. *Cerebral cortex*, 12(9):908–914, 2002.

[49] Simone Vossel, Joy J Geng, and Gereon R Fink. Dorsal and ventral attention systems: distinct neural circuits but collaborative roles. *The Neuroscientist*, 20(2):150–159, 2014.

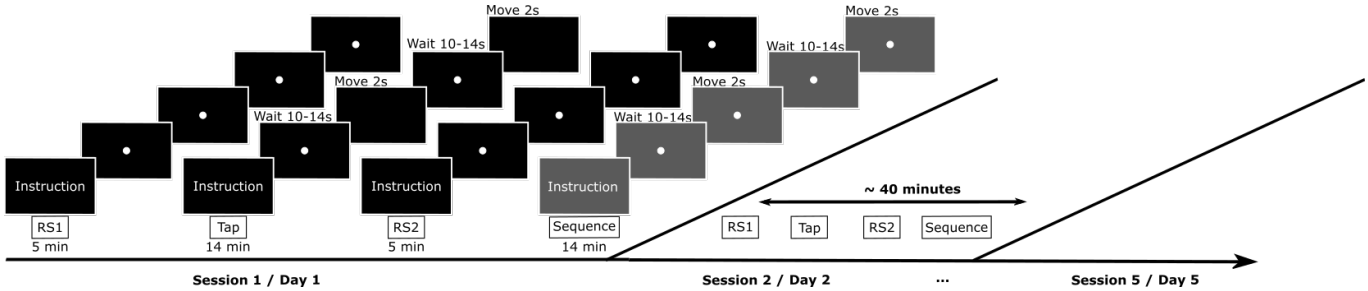

Fig 1. Experimental Paradigm. Figure showing the experimental conditions. Top: Single measurement sequence consisting of 5 min Resting State (RS1), 14 min Tapping Task (Tap), 5 min Resting State (RS2), and, finally, 14 min Sequence Task (Sequence). The sequence task is shown in grey as it will not be considered for further analyses; Bottom: Temporal sequence of measurements for day 1 to day 5.

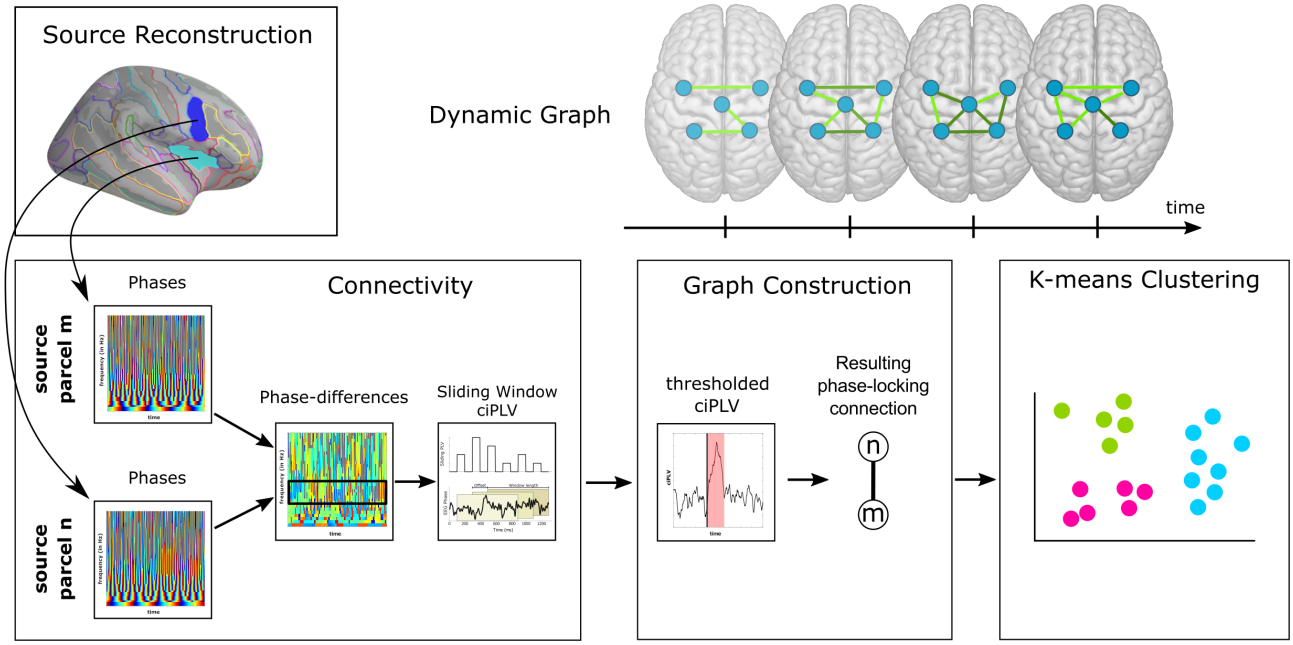

Fig 2. Connectivity State Pipeline. Representation of how the connectivity states were determined. Top row (left): extraction of source activity for two parcels, m and n; bottom row (left): computation of the ciPLV connectivity metric; bottom row (middle): graph construction for each time window by thresholding the ciPLV; top row (right): depiction of the resulting dynamic graph networks; bottom row (right): application of k-means clustering for connectivity state assignment.

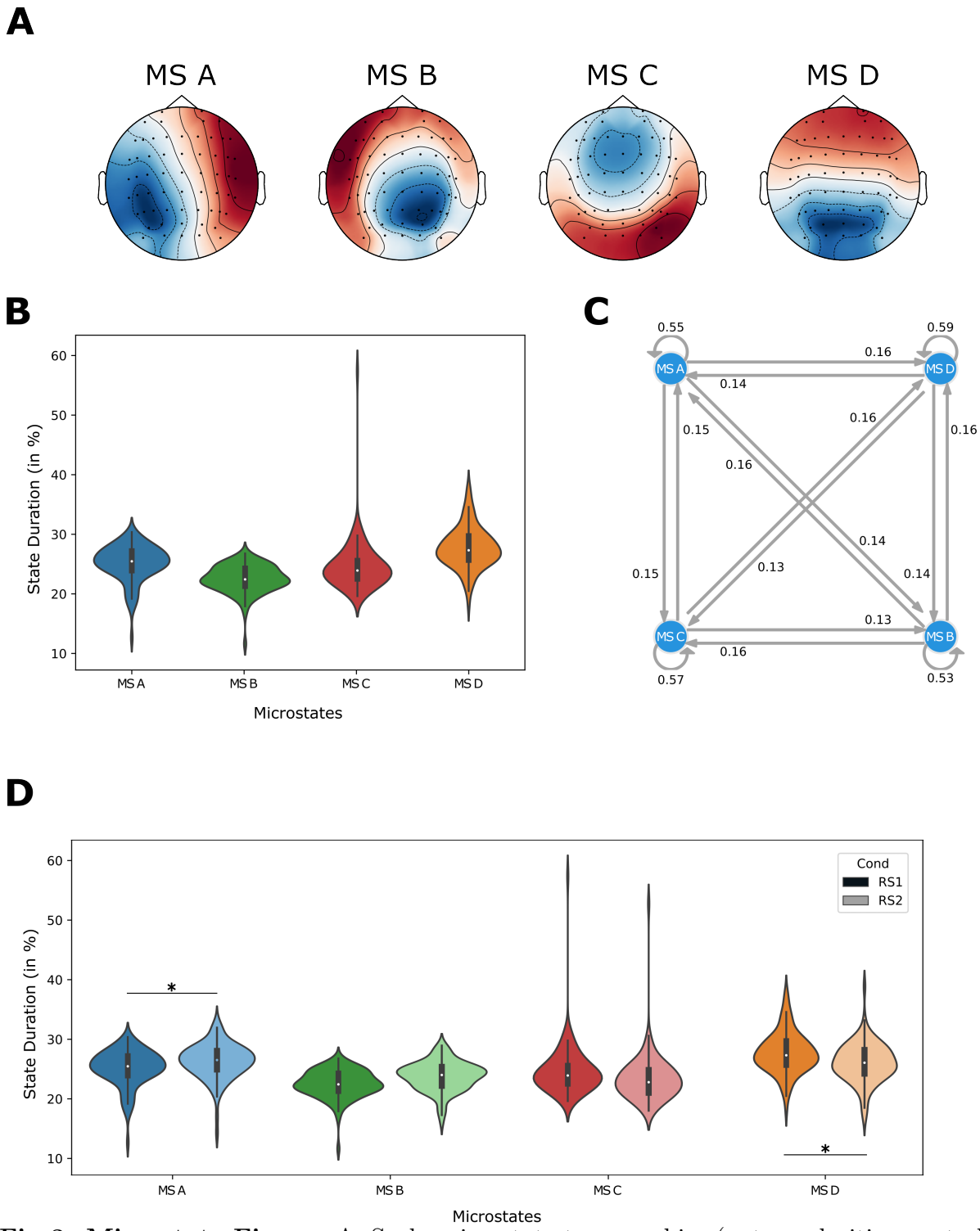

Fig 3. Microstate Figure. A: Scalp microstate topographies (note: polarities are to be neglected), B: relative time the brain stays in each state, C: transitions between the four microstates displayed as a Markov diagram (A-C: all subjects, all sessions, RS1 only), D: comparison of RS1 and RS2 state durations (all subjects, all sessions), darker tone representing RS1 lighter tone RS2 respectively.

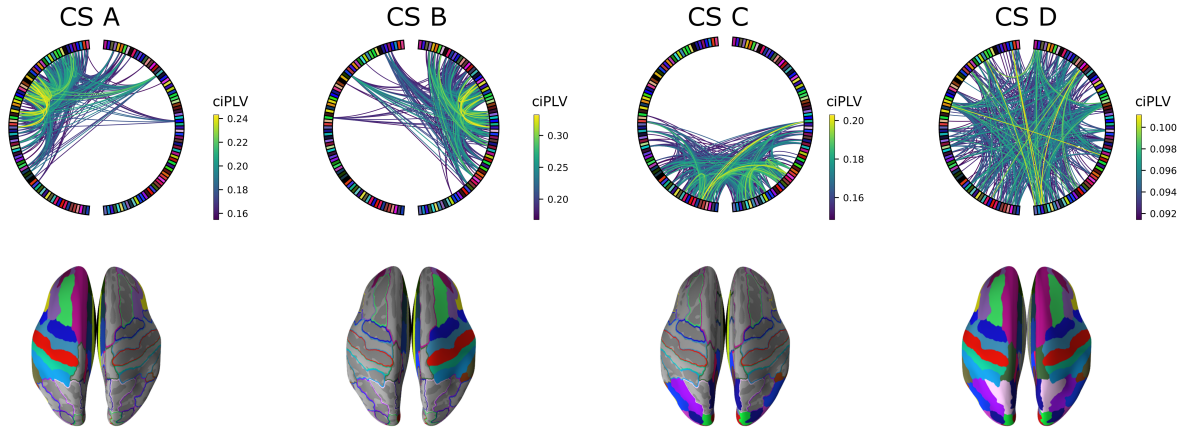

Fig 4. Source Connectivity States. Top: circular presentation of source connectivity (10% strongest connections shown) presenting parcels on each hemisphere on the left and right side of the circular plot, frontal parcels at the top and occipital parcels on the bottom; Bottom: presentation of the involved parcels mapped onto the brain using the same color code as in the circular plot.

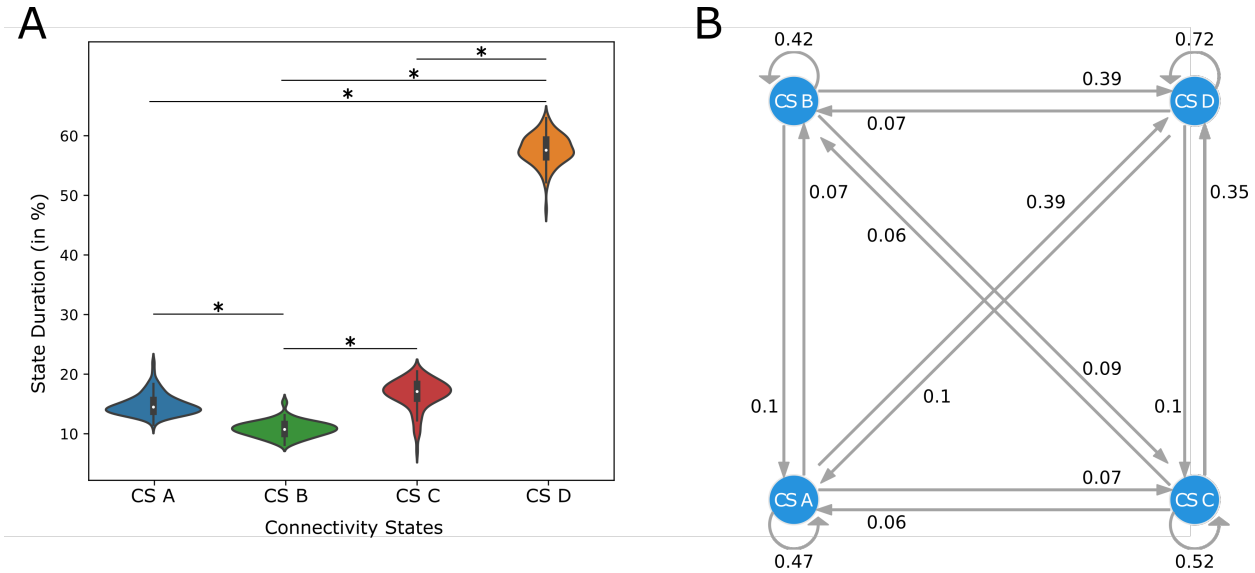

Fig 5. Durations and Transitions of Source Connectivity States. A: A violinplot showing the source connectivity state durations for CS A (blue), CS B (green), CS C (red) and CS D (orange) in RS1. All significant differences are marked with an asterisk; B: graph displaying the transitions between the connectivity states.

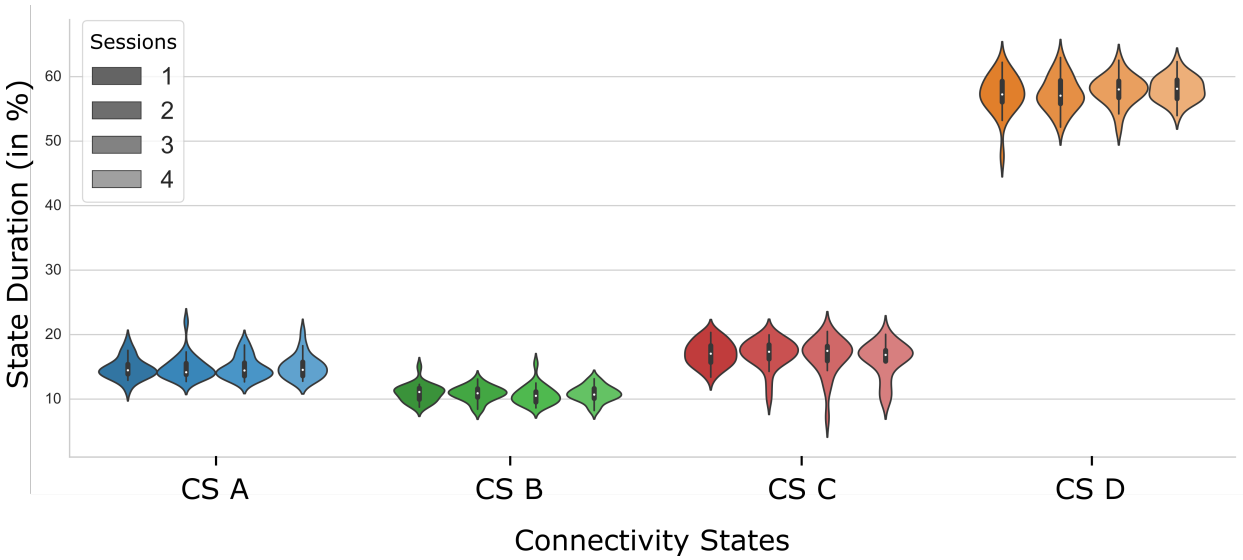

Fig 6. Connectivity States for multiple measurement days. A violinplot showing the source connectivity state durations for separate measurement days, i.e. sessions; color coding representing sessions 1 (darkest) to 4 (lightest).

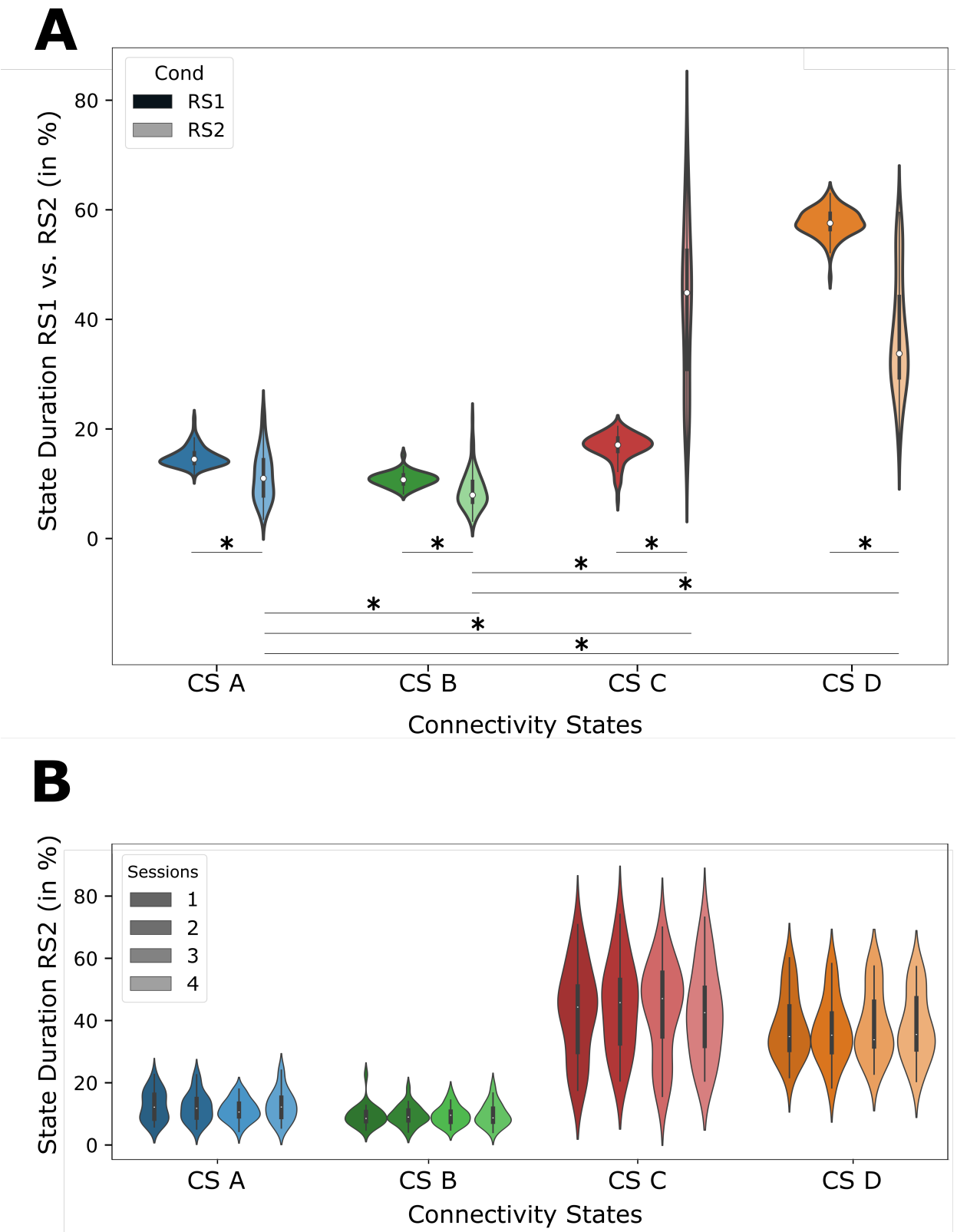

Fig 7. Task-dependent changes in connectivity states. A: A violinplot showing the source connectivity state durations separately for RS1 and RS2 (all sessions); B: Stability of source connectivity state durations in RS2 for multiple measurement sessions; color coding representing sessions 1 (darkest) to 4 (lightest).

Supplementary Material

Previous motor task performance impacts phase-based EEG resting-state connectivity states

Nils Rosjat[1], Maximilian Hommelsen[1], Gereon R. Fink[1,2], Silvia Daun[1,3,*]

1 Cognitive Neuroscience, Institute of Neuroscience and Medicine (INM-3), Forschungszentrum Jülich, Jülich, Germany
2 Medical Faculty, University of Cologne, and Department of Neurology, University Hospital Cologne, Cologne, Germany
3 Institute of Zoology, University of Cologne, Cologne, Germany

S1 - Microstate topographies remain stable over measurement sessions In the main text, we presented the four MS topographies as defined by all four sessions combined. To check whether these states are stable across all measurement sessions and between RS1 and RS2, we performed the MS clustering separately for each measurement day. When comparing the MS topographies in the main text (Fig. S1, first row, RS1) with the other four MS topography configurations (second to fifth row, session 1 - 4, RS1) and RS2 (sixth row), there is a high level of similarity with only minor changes in the MS topographies. Therefore, we can assume that the MS topographies do not change significantly over the measurement days.

S2 - Connectivity state analysis for 8 states Besides to the classical analysis defining 4 microstates, we clustered the data into 8 micro (MS)- and 8 connectivity states (CS). The results are presented in Fig. S2. We generally observed similar phenomena as in the results presented in the main text. MS analysis showed almost equally distributed states which were stable across measurement days (Fig. S2B and C). In the CS analysis, we found 5 states (CS A, B, C, G, and H) that occurred roughly 10% of the time, while three other states showed an increased duration of 15% (CS E), 20% (CS F) and 28% (CS D). The same behavior could be observed when dividing the data into measurement sessions. When examining the patterns of MS and CS, it is noticeable that there are remarkable similarities to the phenomena described in the main text (e.g., MS E-H or CS C, E, and G). Besides the patterns already described, 4 other patterns appeared, which in some cases (such as MS D and MS H or CS A and CS C) were in part very similar to each other, and thus one should be careful in arguing that they represent new/independent states.

S3 - Source reconstruction - motor task To ensure the validity of the source localization in the resting states, we first performed a localization of the motor activity during finger movement in the "Tap" task. As shown in Fig. S3, there is an increase in activity in the area of the primary motor cortex during finger movements. Furthermore, we used this experimental condition to determine the best possible parcellation for our data. The aim was to map the activity to as fine structures as possible, which are close to the course of the source activity, but not to determine too many sources simultaneously since only 61 underlying EEG recordings were available. While the Desikan-Killany atlas and the Brodmann parcellation are coarse and not close to the observed activity, the sub-parcellation of the DKT atlas clearly defines too many sources. The Destrieux atlas is close to the observed activity and has hardly more parcellations than the Brodman atlas. Thus, we selected the Destrieux parcellation for our further investigations.

S4 - Source connectivity - resting state This figure provides a comprehensive exemplary view of the mean corrected imaginary phase-locking value (ciPLV) across all subjects, sessions, and time windows for each pair of source parcels under investigation. The purpose of this figure is to demonstrate the existence of varying strengths of connectivity throughout the entire network, indicating that the connections between these parcels are not zero. This observation is crucial as it signifies the presence of meaningful connectivity within the network. By illustrating the non-zero connectivity, this figure supports the notion that the networks formed based on these connections carry significance and are not mere random or spurious associations.

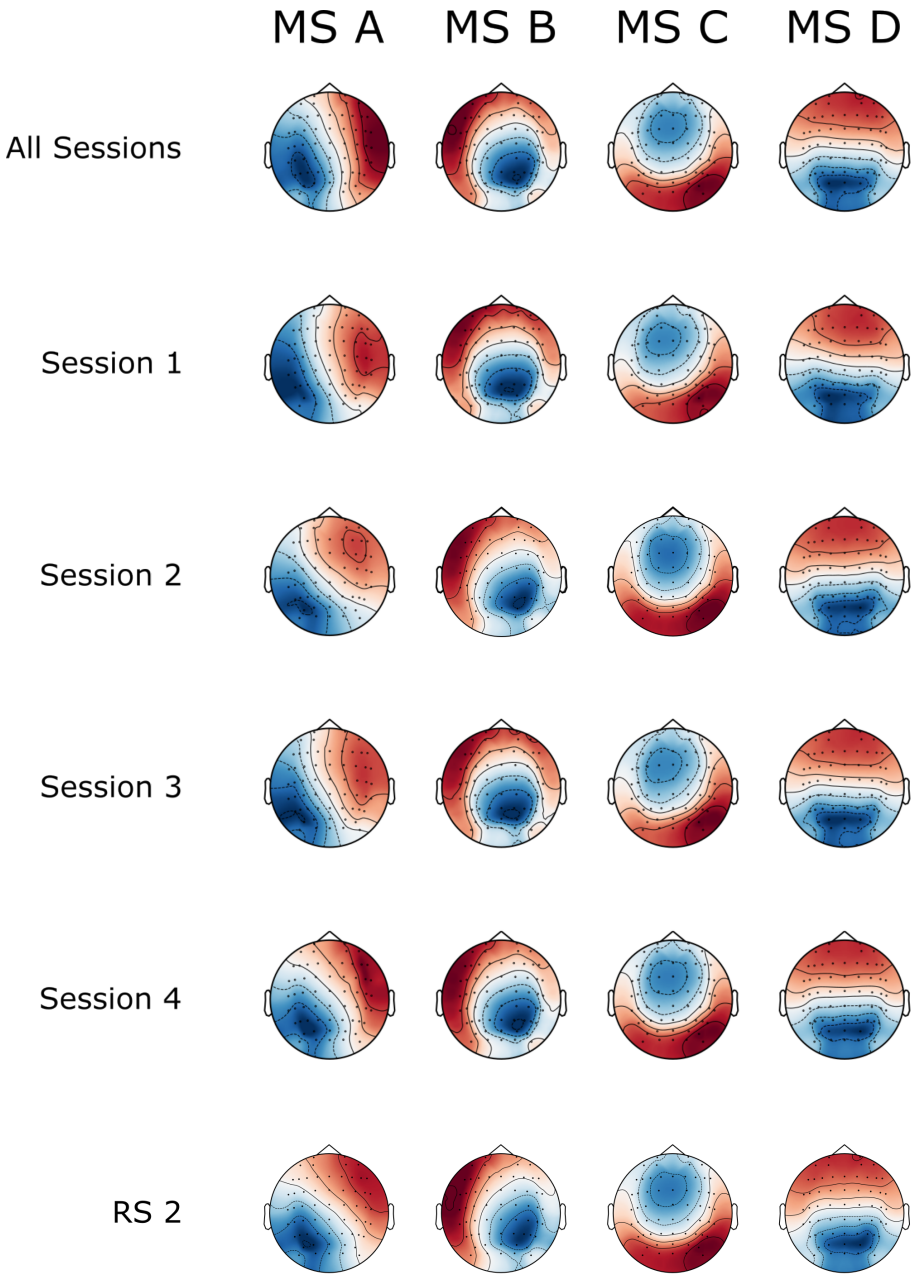

Fig S1. MS topographies remain stable over measurement sessions. Microstate topographies analyzed separately for different measurement days. First row: MS topography for all sessions as shown in the main text (RS1); Second row: MS topography for session 1, RS1; Third row: MS topography for session 2, RS1; Fourth row: MS topography for session 3, RS1; Fifth row: MS topography for session 4, RS1; Sixth row: MS topography for RS2, all sessions.

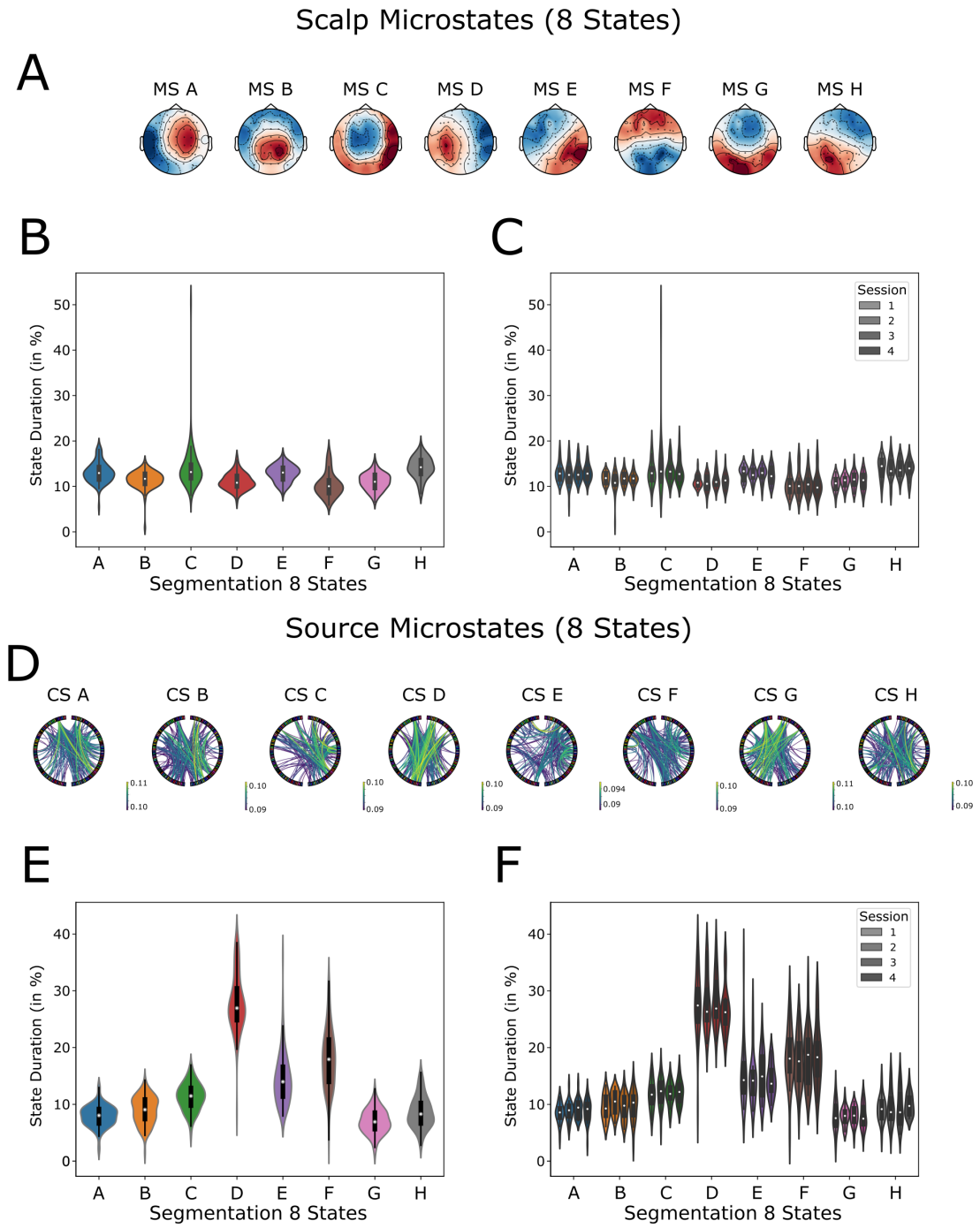

Fig S2. MS and CS analysis for 8 states. Microstate analysis (A-C) and source connectivity state analysis (D-F) for 8 states in RS1. A: MS A-H topographies; B: MS duration for MS A-H; C: MS duration for MS A-H for different measurement sessions; D: CS networks for CS A-H; E: CS duration for CS A-H; F: CS duration for CS A-H for different measurement sessions.

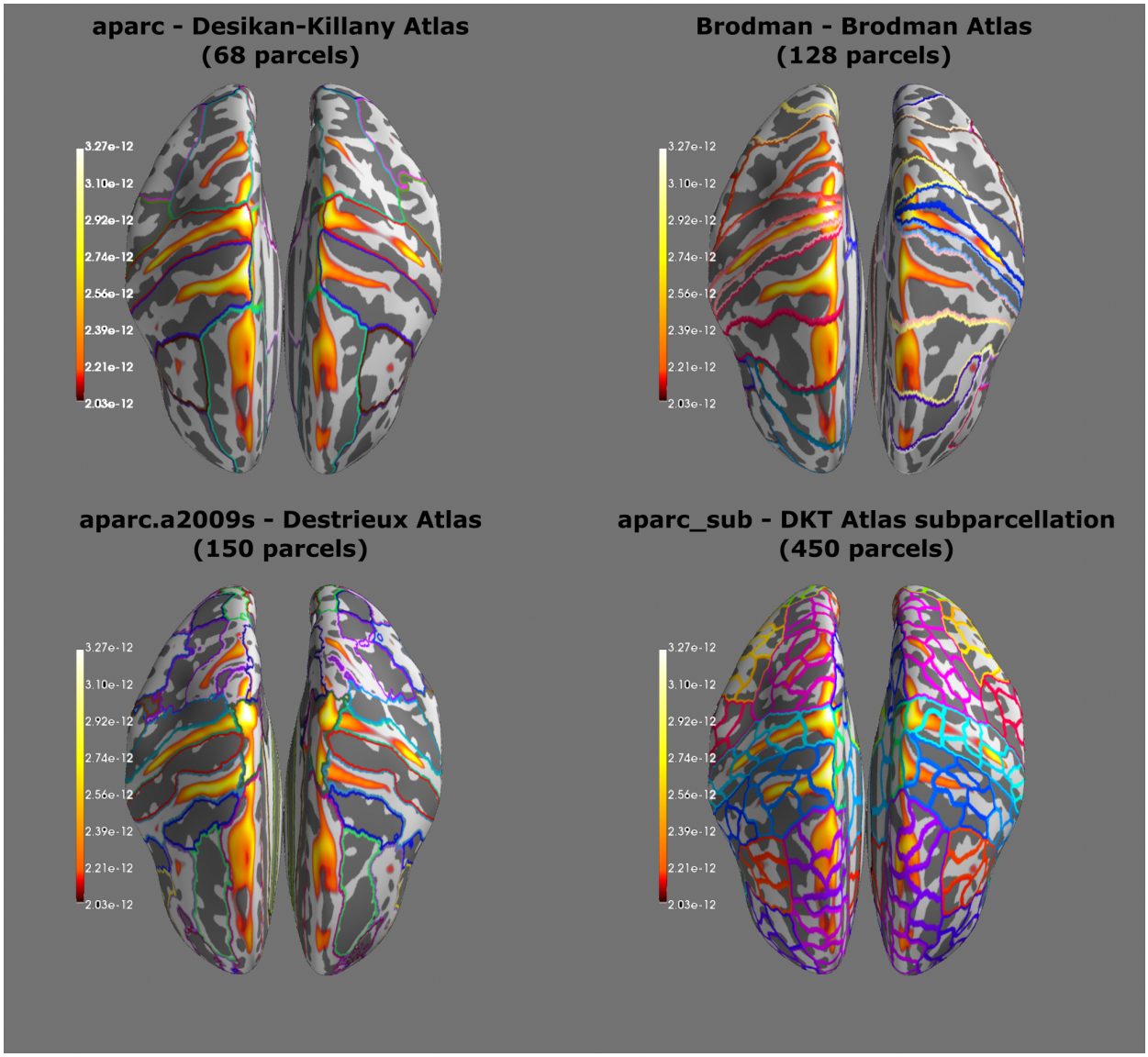

Fig S3. Source reconstructed activity for finger tap movement. Source reconstructed motor activity for four different types of cortical parcellations. Top left: Desikan-Killany atlas; Top right: Brodmann atlas; Bottom left: Destrieux atlas; Bottom right: DKT atlas subparcellation.

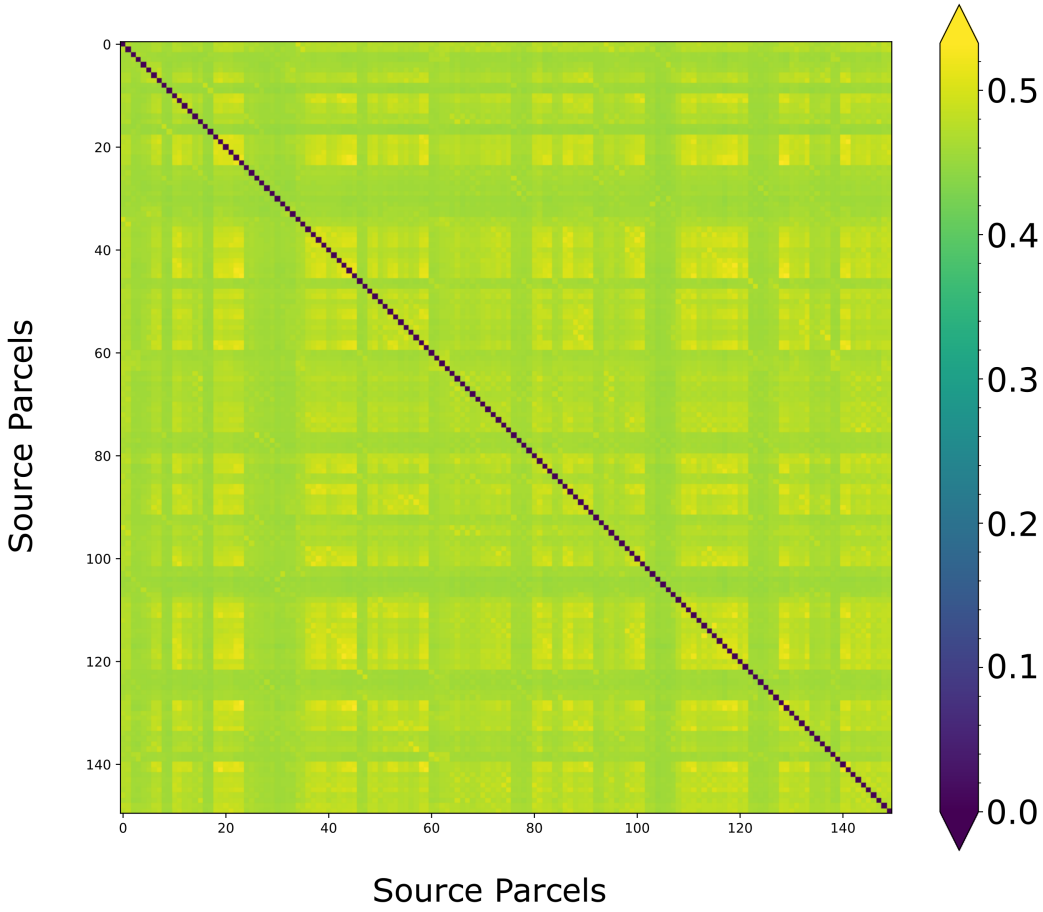

Fig S4. Source ciPLV. Mean ciPLV over all subjects, sessions, and time windows of RS1 and RS2 for all pairs of source parcels in consideration.